

3. MAGNETS

3.1 Acceptance Criteria

The confluence of test results on more than 170 full-scale magnets¹ that have been built and tested at Fermilab and the accelerator-design work discussed in the remainder of this report, especially the correction and adjustment elements discussed in Section 7, has led to a set of acceptance criteria for dipole magnets. These criteria are given in Table 3-I on the next page.

Both dipole and quadrupole designs are based on extensive computer studies of the magnetic field. We include as Appendix III computer-generated magnetic-field data for both dipoles and quadrupoles.

3.2 Dipole Design

Parameters and specifications of the dipole magnet are given in Table 3-II. Figures 3-1, 3-2, and 3-3 are cross-section views of the dipole, 3-1 showing the over-all magnet, 3-2 the detail of the collared-coil assembly, and 3-3 the end of the cryostat, in particular the helium and nitrogen connections and the helium-pressure relief system. Figure 3-4 is an elevation view, showing the details of the beam tube and cryogenic-fluid connections.

The magnet is a cold-bore, warm-iron design with a two-shell $\cos\theta$ -type coil around a circular bore. The beam tube is slightly flattened into a four-sided cross section, as can be seen in Fig. 3-1. This gives better helium flow where needed between the beam tube and the coils.

The superconducting cable is formed into a keystone cross section during winding. The inner coils are wound flat, then pressed into a saddle shape around a mandrel. The outer coils are saddle wound. The return

Table 3-I. Dipole Acceptance Criteria.

<u>Quench Current</u>	> 4350 A @ ≥ 200 A/s	
<u>AC Loss</u>	< 500 J/cycle @ 4000 A and 300 A/s	
<u>Relative Variation of Integral Field</u>	< $\pm 10^{-3}$ about mean @ 2000 A	
<u>Magnetic Vertical Axis</u>	< $\frac{1}{2} \times 10^{-3}$ rad from vertical measured and marked absolute accuracy @ 2000 A	
<u>Outside Physical Dimensions</u>		
Curvature	± 15 mil from nominal	
Flatness and Twist	within 30 mil envelope	
Relative Twist	2 mr	
<u>Integral Multipole Fields (B_n/B_o at 1 in.) at ≥ 2000 A</u>		
	<u>Normal</u>	<u>Skew</u>
Quadrupole	$\pm 2.5 \times 10^{-4}$	$\pm 2.5 \times 10^{-4}$
Sextupole	$\pm 6.0 \times 10^{-4}$	$\pm 2 \times 10^{-4}$
Octopole	$\pm 2 \times 10^{-4}$	$\pm 2 \times 10^{-4}$
Decapole	$\pm 2 \times 10^{-4}$	$\pm 2 \times 10^{-4}$
<u>Hipot</u>		
Coil, bus, heater to ground	< 5 μ A @ 5 kV	
<u>Electrical Parameters</u>		
(acceptable tolerance about mean)	R $\pm 0.3\%$ (dc)	
	C $\pm 10\%$	
	L $\pm 2\%$ (at 1 kHz)	
	Q $\pm 10\%$ (at 1 kHz)	
<u>Vacuum (maximum leak room temp.)</u>	5×10^{-9} atm-cc/s	

YOKE DIMENSIONS (In.):

Inner Radius: 3.765
Width: 15
Height: 10
Maximum Twist: $\pm 1/32$
Sagitta: 0.26

LENGTHS (In.):^a

Yoke: 235
Inner Coil:
To Inner Radii: 238.5
To Outer Radii: 245.115
Outer Coil:
To Inner Radii: 241.474
To Outer Radii: 244.635
Cryostat (to interface): 252

COOLING:

Helium:

1 ϕ capacity: 15 l/magnet
2 ϕ capacity: 7.1 l/magnet
1 ϕ inlet: 4.5 K
(1st magnet)
1 ϕ outlet: 4.6 K
(22nd magnet)
2 ϕ inlet: 4.47 K
(22nd magnet)
2 ϕ outlet: 4.42 K
(1st magnet)
Helium flow rate: 20.55 g/s

Nitrogen:

LN capacity: 6.7 l
Max. temp.: 85 K
(outlet)

WEIGHTS:

Collared Coil Assembly	1050 lb
Cryostat	550
Yoke	<u>6800</u>
Total	8400

^a See drawing 1620-MB 103657A

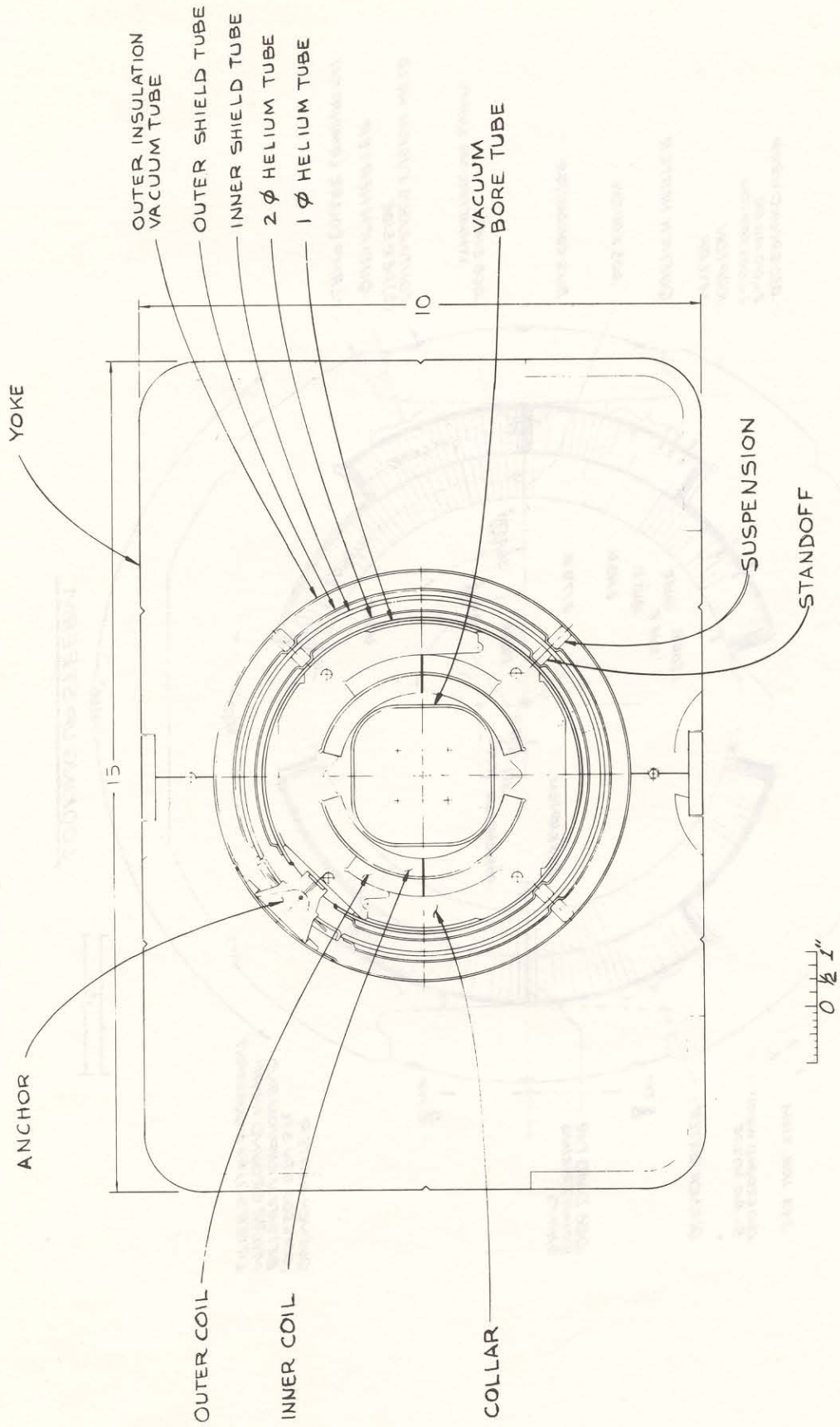


Fig. 3-1. Cross section of dipole magnet.

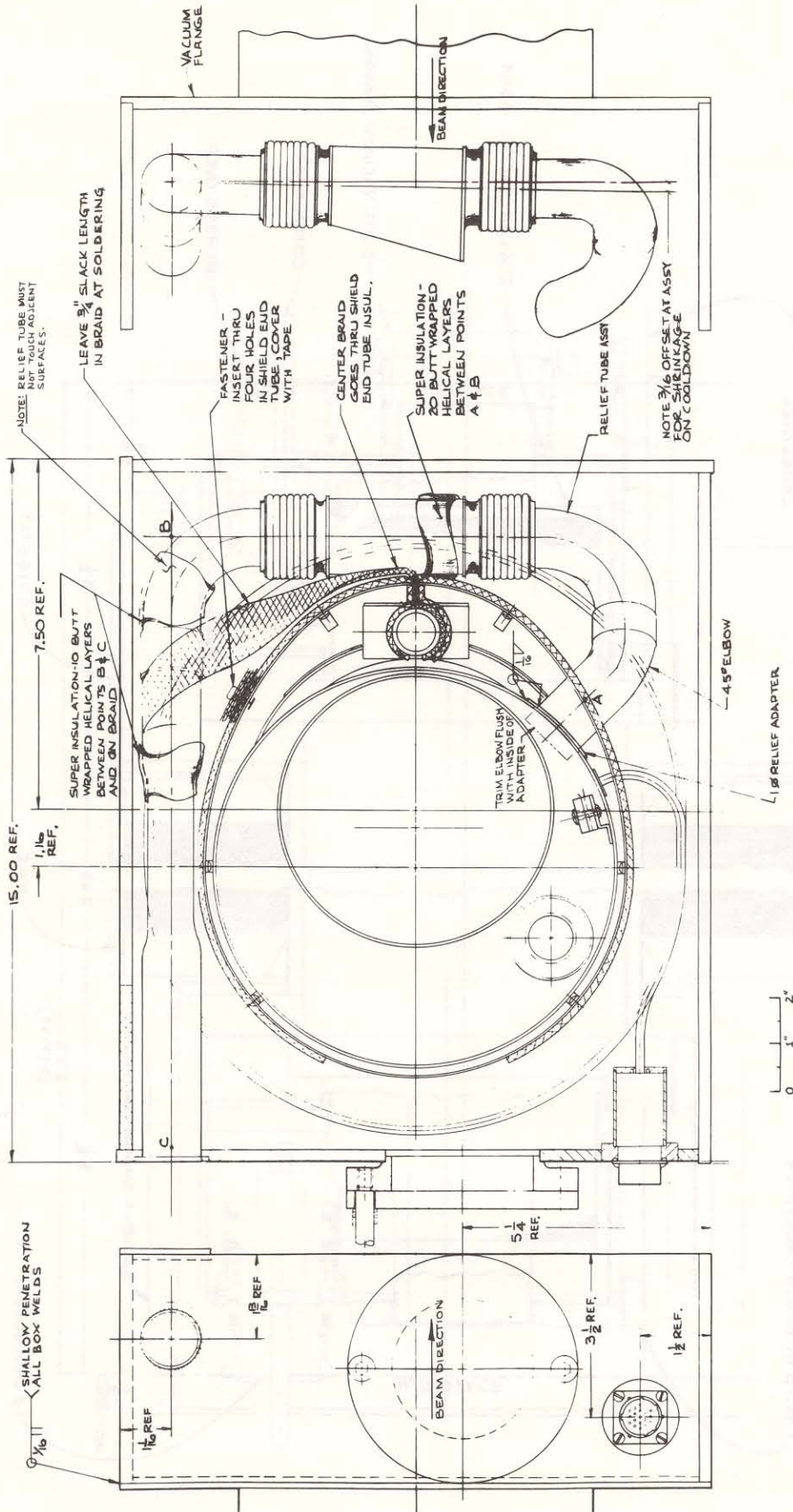


Fig. 3-3. Cross section of dipole cryostat.

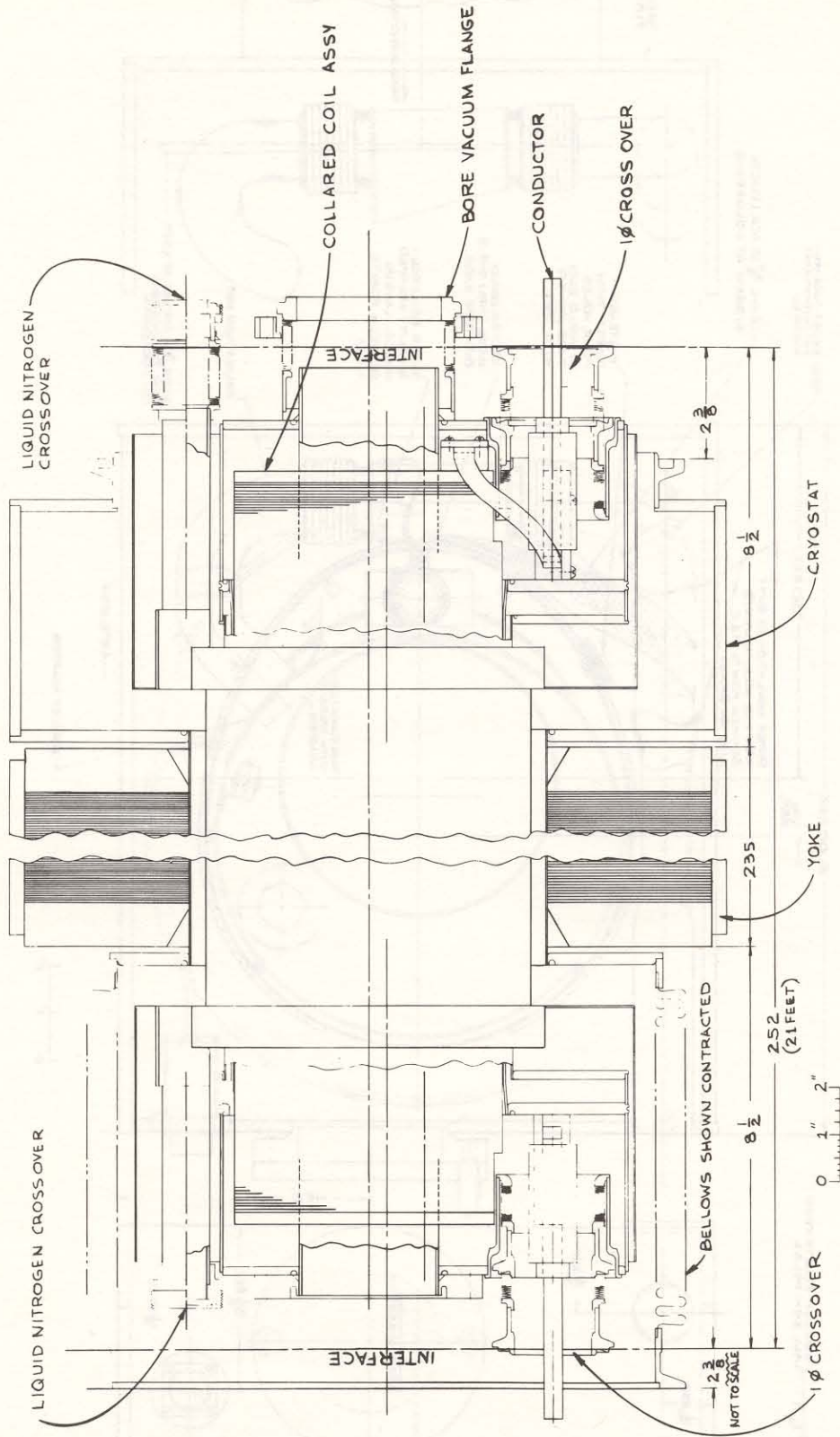


Fig. 3-4. Longitudinal cross section of dipole magnet.

bus and stainless-steel heater coils are wound integrally with the coils. The heater coils are fired when a quench is detected, as discussed in Section 6, to quench all the magnets in a half-cell as a unit and distribute the stored energy of the field to avoid damage.

The coils are held tightly in place against their own magnetic forces by the laminated two-piece stainless-steel collars shown in Fig. 3-2. The individual collars are formed into separate 4-in. upper and lower packs, which are assembled around the coils, then compressed in a press to give the pre-loading. The compressed collars are welded to complete the collared-coil assembly.

Room-temperature magnetic-field measurements are carried out on this assembly, using approximately 10 A in the coils, a multiple-loop stretched-wire pickup coil and a lock-in amplifier system to measure the normal relative multipoles of the coil.² The values measured in this way are not identical to those measured in the full-scale superconducting measurements discussed below in Section 3.4. The steel yoke adds a little more than 20% to the dipole field and also makes a change in the sextupole component. The quadrupole, octopole, and decapole components agree in the two systems to reasonably good accuracy. With this correspondence understood, the room-temperature measurements can be used to provide rapid feedback to monitor the production process.

Cooling is by single-phase liquid helium with two-phase counterflow heat exchange. Subcooled liquid helium is delivered to the coil space at 24 feed points around the ring and flows away from the feed points in both

directions. Halfway to the next feed point, the liquid passes through a Joule-Thomson valve and flows back through the magnets as boiling helium in thermal contact with the outgoing liquid-helium stream. Heat generated by the coils is transferred to the single-phase liquid, which has relatively high specific heat and heat transfer, and is transferred by it to the colder two-phase reverse flow. Both streams remain at near-constant temperature throughout their paths; heat is absorbed by changing liquid to gas. The refrigeration system external to the magnets is discussed in Section 4 below. Figure 3-1 shows the cryostat in cross section. The standoffs shown are of G-10. The heat leak is measured to be approximately 7 W per dipole.

The complete cryostat is installed in a laminated steel yoke. A wire-loop pickup coil built into the yoke is used to align the cryostat in the yoke, using small currents at room temperature. The yoke assembly has a 0.26-in. sagitta (barely visible) to curve the magnets to fit the orbit.

Considerable experience has been gained by now in fabrication and assembly of all the components of a magnet. One of the important lessons has been the necessity for the strictest quality control at every stage of the process and we have instituted rigorous 100% inspection procedures. It is only by following such procedures faithfully that it is possible to build superconducting magnets with reproducible fields.

The dipole bore is 1.5 in. in radius, with a slightly smaller constriction arising from the squared-off beam tube. The field drops off rapidly beyond a radius of 0.8 in. Such a field is of course rich in multipoles. In particular, the sextupole and decapole are relatively large and

opposite in sign. The magnet ends also contribute significantly to these two harmonics and this contribution is difficult to compute precisely. Adjustment of the angles subtended by the inner and outer coils in the collars, using shims, is used to cancel the body and end sextupole and decapole fields.³ Significant quadrupole fields, both normal and skew, can arise from misalignment of the coils within the yoke and special care is required in assembly.

3.3 Quadrupole Design

Figure 3-5 is a cross-section view of the quadrupole.⁴ Figure 3-6 is an assembly drawing and Fig. 3-7 is a sketch showing the complete quadrupole "spool" assembly with correction coils and the beam detector. Parameters and specifications of the quadrupole are given in Table 3-III.

Table 3-IV gives parameters of the spool package and Table 3-V gives parameters of the correction-element package.

The quadrupole is a cold-bore, two-shell design of 3.5-in. bore. This diameter is chosen to ensure that the quadrupole is not the limiting aperture of the accelerator. There are two coil sections, separated by a spacer, in the inner shell and one section in the outer shell, as shown in Fig. 3-5. The spacer improves the 20-pole of the quadrupole to a negligible value, at the cost of a 10% increase in length to maintain the required integrated gradient. The thickness of the spacer also controls the 12-pole. A change in thickness of the spacer by ten mils (0.010-in.) changes the 12-pole/quadrupole ratio by about 5×10^{-4} at 1 in.

The following comments concern the design of the ancillary features:

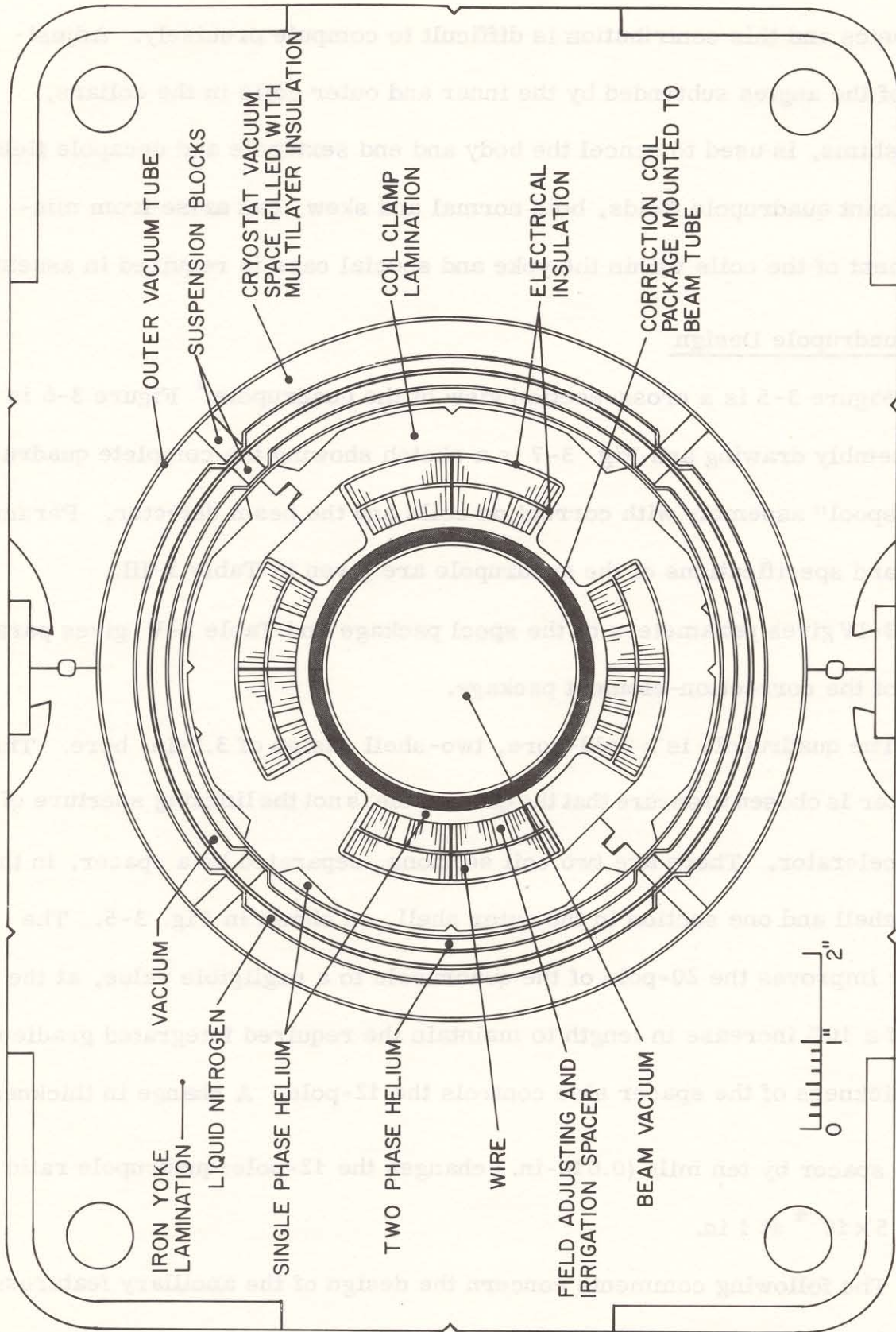


Fig. 3-5. Cross section of quadrupole magnet.

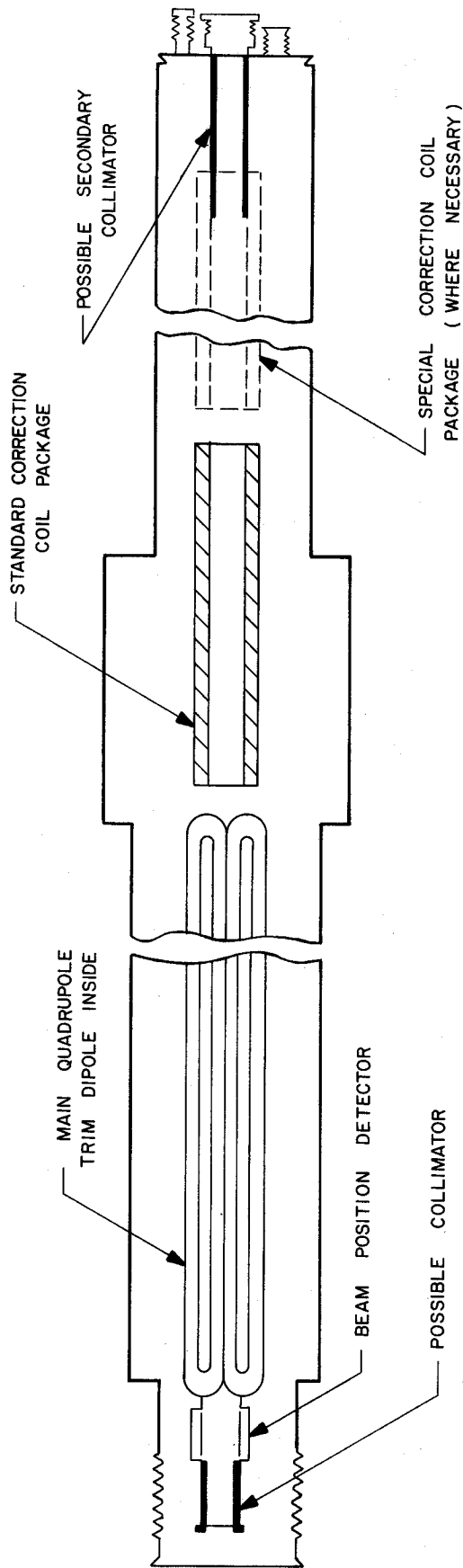


Fig. 3-7. Longitudinal cross section of quadrupole and correction coil assembly.

Table 3-III. Type Q Quadrupole Coil/Cryostat Parameters and Specifications.

	<u>Inner Coil</u>	<u>Outer Coil</u>	
Inner Radius	1.750	2.088	in.
Outer Radius	2.067	2.405	in.
Key Angle	30.1194	30.7839	deg
No. Turns	14	20	
Conductor Required	210 (×4)	280 (×4)	ft
Assembly Dimensions (all in in.):			
Outer Collar Radius:	2.933		
Ground Wrap Material/Thickness:	Kapton/0.028		
Coil Length (Actual):	69		
Coil Length (Magnetic):	66.1		
Yoke Length:	63		
Yoke Inner Radius:	4.000		
Yoke Outside Dimension:	9.750 × 15.478		
Overall Slot Length:	163		
	<u>Inside Radius</u>	<u>Material Thickness</u>	
	(In.)	(In.)	
Beam Tube	1.372 (3.485 cm)	0.065	
1 Phase Tube	3.040	0.036 (20 GA)	
2 Phase Tube	3.177	0.036 (20 GA)	
Inner Shield Tube	3.389	0.049 (18 GA)	
Outer Shield Tube	3.552	0.036 (20 GA)	
Vacuum Tube	3.963	0.036 (20 GA)	

(i) Vacuum Break. A preliminary design for a vacuum-isolation scheme has been completed as it relates to internal spool components. An external manifold is required to connect upstream and downstream insulating-vacuum regions, assuming redundancy of pumping systems is desired. Although cumbersome, this manifold facilitates the upstream-downstream connection with the proposed break. This external pipe (with valve) is not shown on the assembly drawing.

Table 3-IV. Spool Service Package Parameters and Specifications.

1 Phase Relief:	1 @ 1- $\frac{1}{2}$ in.
2 Phase Relief:	1 @ 1 in.
LN ₂ Relief:	1 @ 3/4 in.
Insulating Vacuum Relief:	1 @ 1- $\frac{1}{2}$ in. 1 @ 5.4 in. ²
Insulating Vacuum Pumpout:	6 in. Conflat
Thermocouple Flanges:	1 - KF - 10 1 - KF - 40
Beam Vacuum Sniffer:	2-3/4 in. Conflat termination
Beam Position Monitor:	1 @ 6 in. length, upstream end
Safety Lead:	1 lead, Constantan, 0.3916 in. ² cross section, 8 ft length, connected to quadrupole coil lead
1 Phase Instrumentation:	100 Ω carbon resistor for temperature measurement, bus/coil voltage taps
Correction Element Power Leads:	10 vapor-cooled leads @ 75 A for correction packages

Table 3-V Correction-Element Package Parameters and Specifications.

	2P	4P	6P	8P
Inner Diameter	2-7/8 in.	3-7/8 in.	3-7/16 in.	3-1/16 in.
Outer Diameter	3-1/32 in.	4-1/16 in.	3-3/4 in.	3-5/16 in.
Coil Length (maximum)	65 in.	30 in.	30 in.	30 in.
Magnetic Length	62 in.	27 in.	27 in.	27 in.
No. Layers	4	4	7	6
No. Turns	330	220	220	120
Nominal Current	50 A	50 A	50 A	50 A
Self Field	0.32 T	0.44 T	0.45 T	0.47 T
% Field Due to Iron	a	42	23	5
Nominal Strength @ 1 in.	175 kG-in.	61 kG-in.	50 kG-in.	30 kG-in.
Estimated Inductance	250 mH	200 mH	200 mH	130 mH
Iron Length	a	30- $\frac{1}{2}$	30- $\frac{1}{2}$	30- $\frac{1}{2}$
Iron Outside Diameter	a	5 in.	5 in.	5 in.

^aSteering dipoles are wound as an integral part of the beam-tube sub-assembly.

(ii) Beam Detectors. The present design of the type Q quadrupole contains one beam detector at the upstream end. It is of the electrostatic type, 6-1/8 in. long, 3-3/4 in. diameter, with a plate separation of 2.557 in. (6.49 cm). A device 8 in. long with a plate separation of approximately 3 in. (7.6 cm) could be accommodated.

(iii) Beam-Loss Shielding. A shield of the kind discussed in Section 13 on the upstream and/or downstream end of the quadrupole package can be easily accommodated. Devices of 3.3 cm o.r. or less and 12-in. length or less should pose no significant problems.

(iv) Feed and Turnaround Region. The single-phase region housing the 30 in. correction package (4P, 6P, 8P) terminates approximately 114 in. from the upstream interface. At regular quad locations 1ϕ , 2ϕ , LN₂, insulating vacuum and beam tube span the remaining 49 in. to the downstream interface (@ 163 in.) at established end-view coordinates. At feed or turnaround locations these lines can be terminated as required in either welded or flange sealed connections.

3.4 Measurements and Results on Dipole Magnets

3.4.1 Training and maximum quench currents. In these measurements, a quench is detected by monitoring the resistive voltage across the magnet. The inductive voltage drop is bucked out by a toroidal coil coupled to the current bus. When a quench is detected, most of the stored energy is dumped by a thyristor switch into an external water-cooled resistance. At full current, only 0.1 MJ of the full 0.5 MJ stored energy is dissipated in the

magnet. We have separately studied dumping the full 0.5 MJ in magnets to test the pressure-relief tube. We have also measured the field changes with quenching and found them to be very small.

With the tight restrictions of the interlocking Type V collars, very little training is needed to reach full field. Magnets usually reach more than 4300 A (4.29 T) at a 200 A/s ramp rate after a few quenches. Figure 3-8 on the next page shows ramp-rate dependence of maximum quench fields.

3.4.2 AC loss. Most of the eddy-current loops have been eliminated by the use of Ebonol-treated strand. The ac loss is now consistently smaller than 500 J/cycle in Ebonol magnets, which is low enough to allow operation with the refrigeration system of Section 4.

3.4.3 Integral fields. The integral fields are measured as a function of excitation by a stretched-wire system. The integral field is approximately 6.409 T-m/kA. Figure 3-9 shows the dependence on excitation and it can be seen that the hysteresis is quite small. The hysteresis is approximately 14 G and saturation of the steel is noticeable above 3000 A. The total effect reaches 20 G at 4000 A.

The stretched-wire system is a difficult measurement and we have therefore recently developed equipment that scans the field through the magnet with a NMR probe and a NMR-calibrated Hall probe for the fringe fields. This system is providing a more accurate absolute integral field as well as the longitudinal structure of the field. An example is shown in Fig. 3-10.

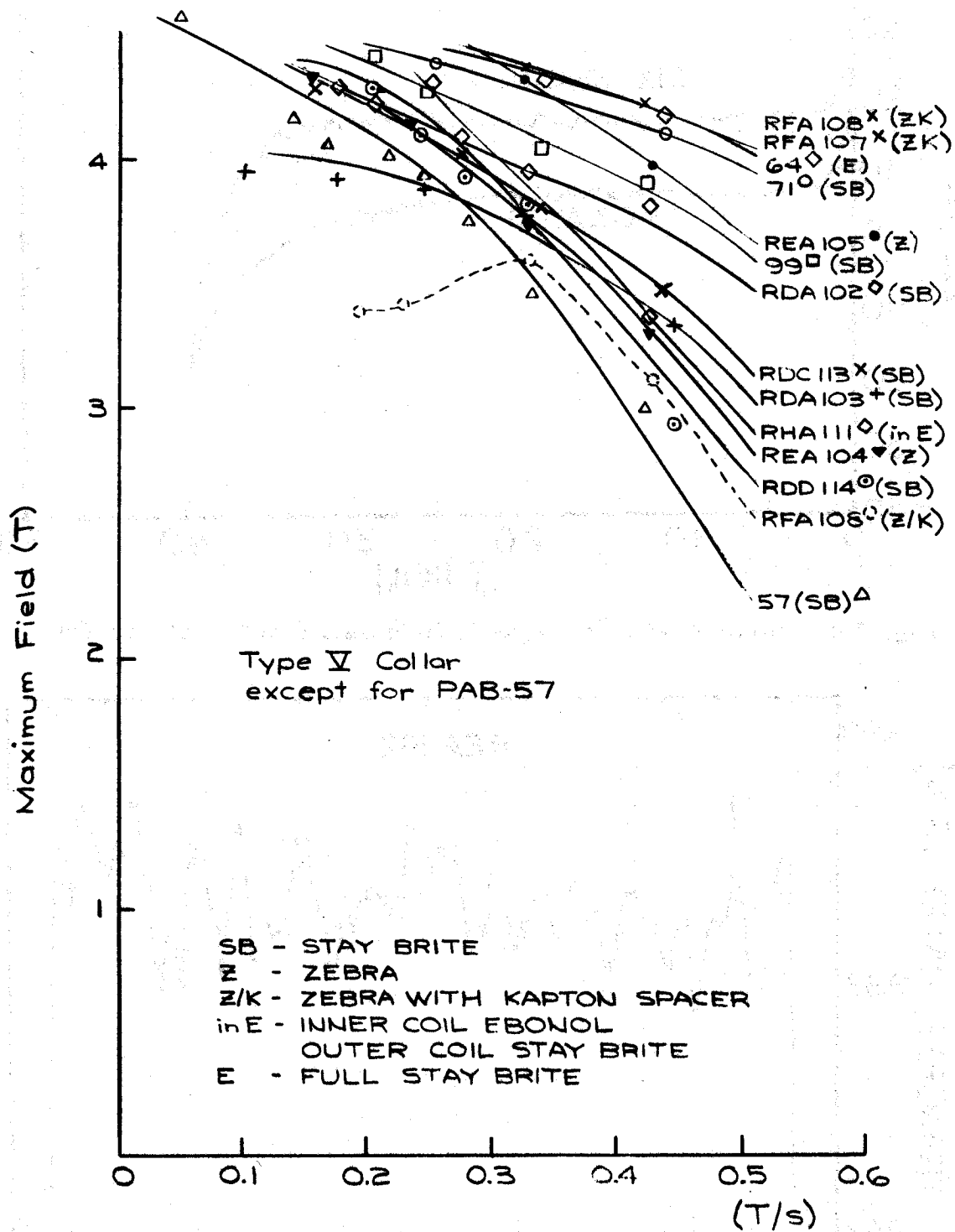


Fig. 3-8. Ramp-rate dependence of maximum quench fields.

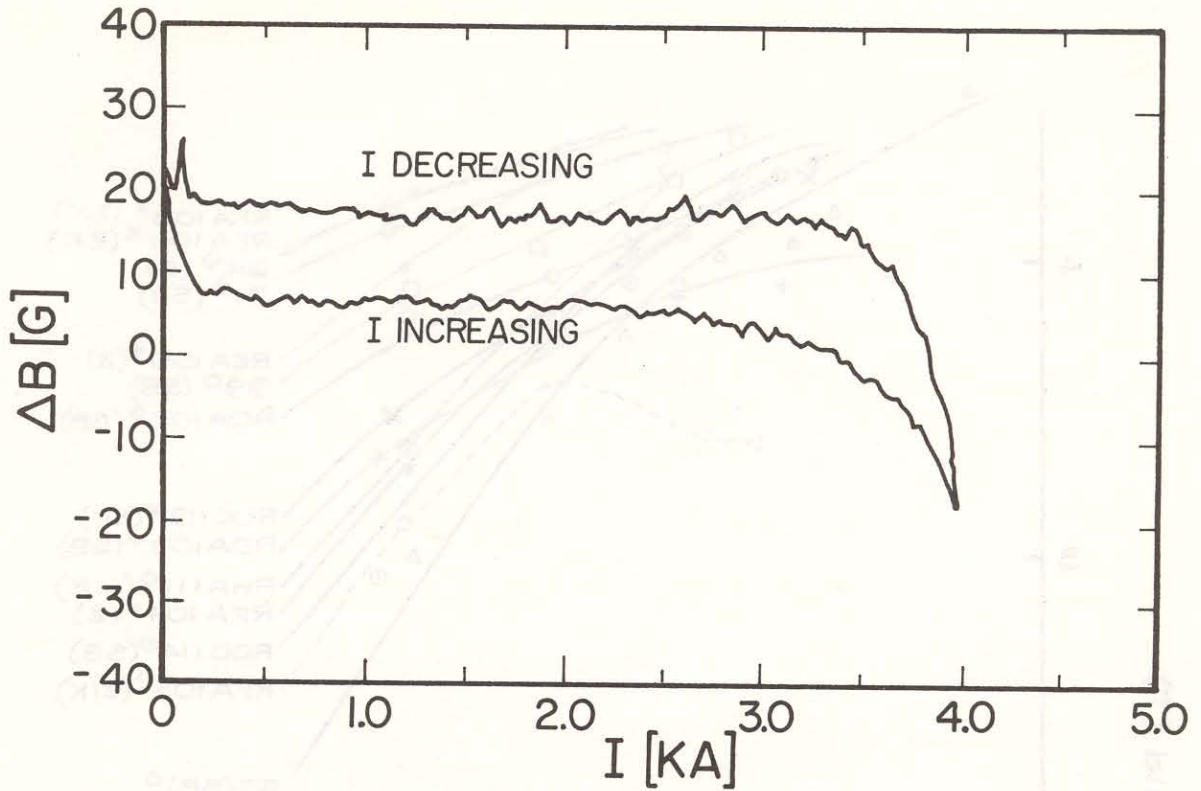


Fig. 3-9. Nonlinearity of magnetic field as a function of current.

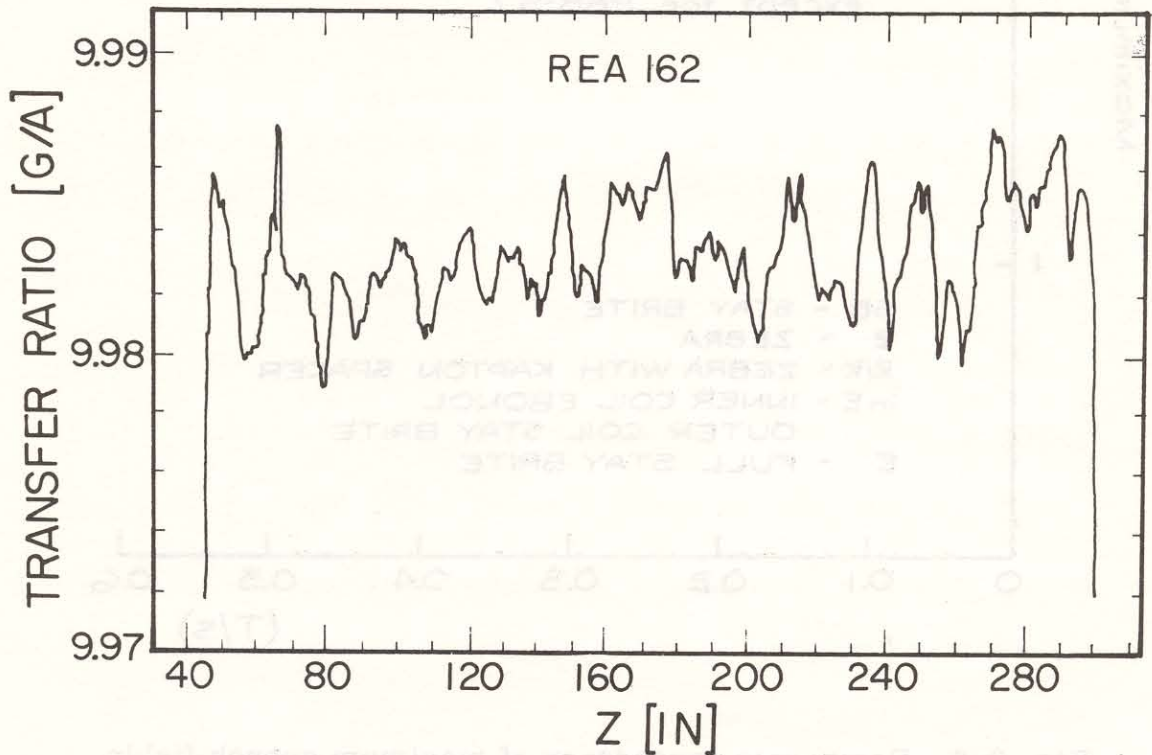


Fig. 3-10. Scan of the transfer ratio of a dipole magnet along its longitudinal axis.

3.4.4 Multipole fields. The field in the beam bore is measured by a harmonic coil. Harmonic components up to the 30th pole are required to give an accurate description of the field.

Our coil is 8 ft long and therefore three measurements are required to cover an entire magnet. Signals are analyzed in real time and transformed to normal (b_n) and skew (a_n) harmonic components, defined as

$$B_y + iB_x = B_0 \sum_{n=0}^{\infty} (b_n + ia_n)(x + iy)^n,$$

where the pole number is $2(n + 1)$. The sextupole and decapole values are used to adjust the key angles of the coils.

There were some difficulties with overpressures in the collaring process partially crushing the small helium irrigation channels located next to the inner-coil keys. The resulting changes in coil dimensions were mirrored in changes in the sextupole. With careful attention to quality control, we are now building production magnets whose multipole components are close to the tolerances of Table 3-I.

Because of persistent currents in superconductors, some multipole components have large hysteresis effects, as shown for the sextupole component in Fig. 3-11, but they are quite reproducible. They are, of course, less important at higher excitations. There are no observable saturation effects on the multipole components, because the steel is far from the coils.

Harmonic components are also measured dynamically with ramping current. Figure 3-12 is a comparison of the sextupole fields at different ramp rates.

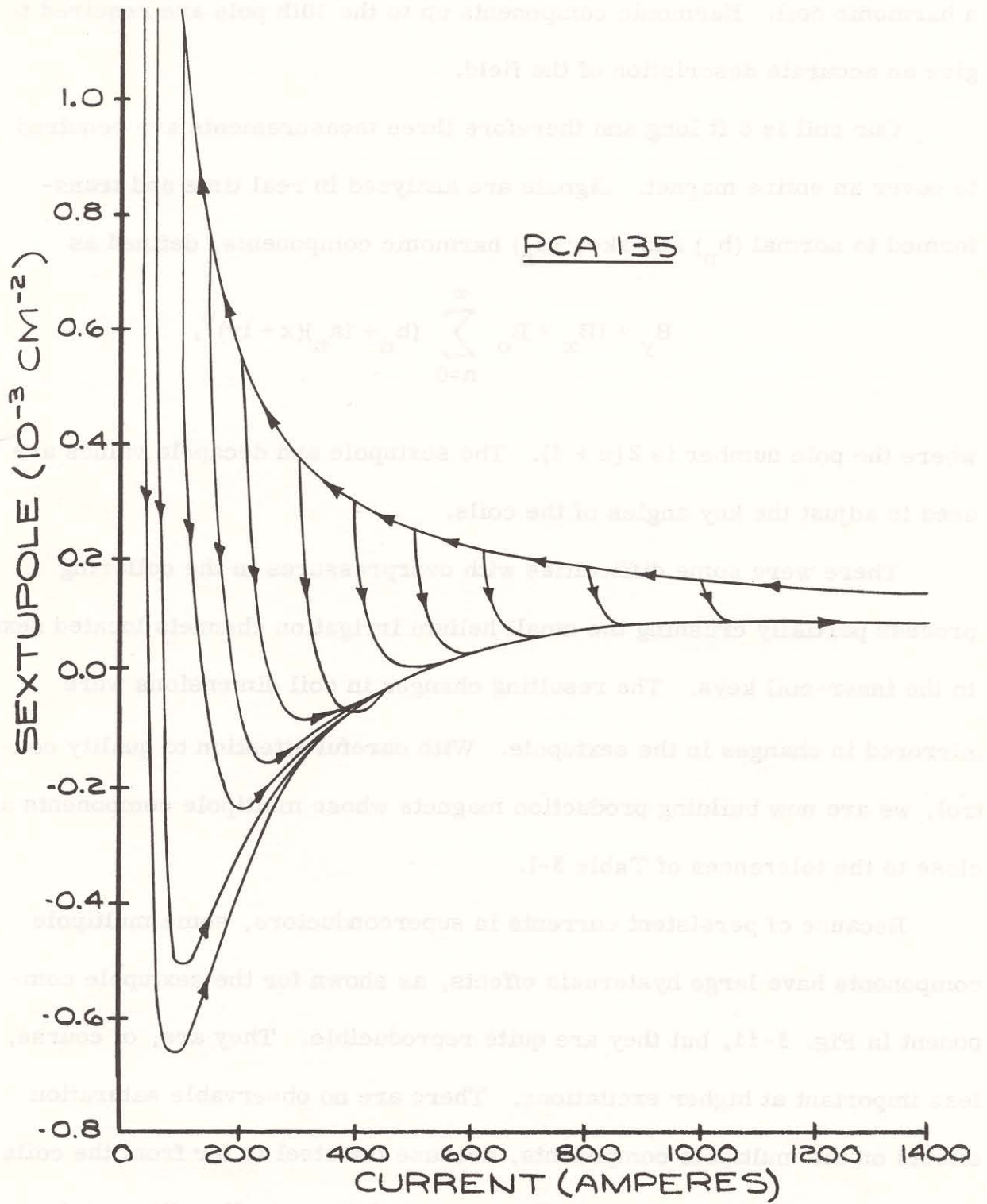


Fig. 3-11. Hysteresis behavior of the sextupole component in a dipole magnet.

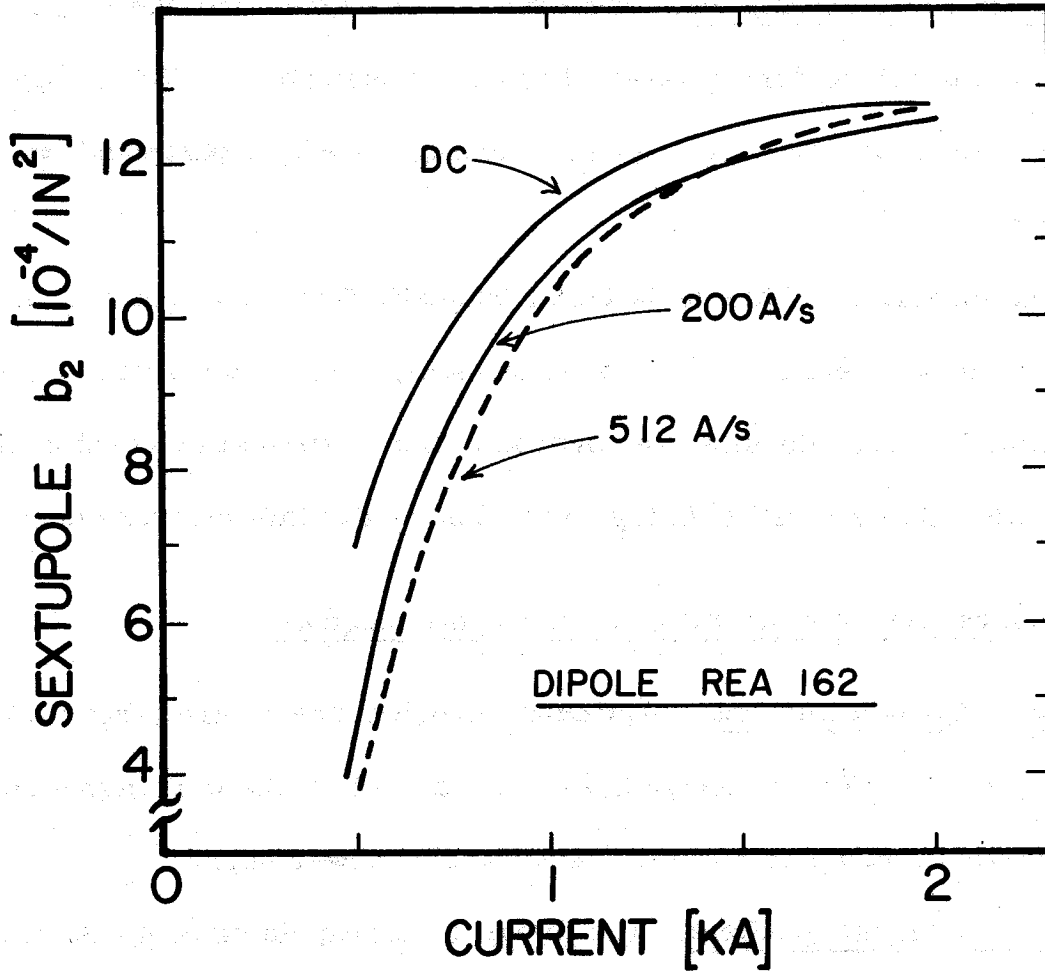


Fig. 3-12. Ramp-rate dependence of the sextupole component in the body field for dipole magnet REA 162.

Here the DC sextupole component is large because the data include only the body field. It has a large positive sextupole, which is to be cancelled by negative sextupole in the end fields.

3.4.5 Field orientation. The cryostat is aligned with the magnet yoke at room temperature during assembly as discussed above. The vertical plane is then measured in the superconducting state by a stretched-wire technique.

The magnitude of the deviation of magnetic from yoke vertical has been of concern to us, because it has major consequences on the sizes planned for correction dipoles. Results are covered in the statistical discussion of Section 3.6. We are still refining our techniques in this measurement.

3.5 Measurements and Results on Quadrupole Magnets

3.5.1 Quench current. Maximum quench currents are large (4.57 kA at a ramp rate of 670 A/s on QB2) and one can only make the magnet quench at the maximum ramp rate of our Test Facility power supply.

3.5.2 Integral gradient. The integral quadrupole strength is measured with twin wire loops stretched through the magnet. The relative difference in area of the two loops is approximately 2×10^{-3} . The integral gradient strength in QB2 is 121.6 T, whereas the design value is 119.6 T.

3.5.3 Multipole fields. The harmonic coil is composed of two main coils and four supplementary bucking coils. A dipole component arises from off-center positioning of the harmonic coil and this dipole component, as well as the quadrupole component, must be suppressed in order that the harmonic coil give workable sensitivity for higher multipoles. Rough reductions of the dipole and quadrupole are done by the two main coils and further reduction to the order of 10^{-4} is achieved with two orthogonal dipole and two orthogonal quadrupole bucking coils.

The harmonic components at 4000 A are given in Table 3-VI below.

Table 3-VI. Harmonic Components of Integral Field Relative to the Normal Integral Quad Field ($\times 10^{-4} / \text{In.}^1 -1^3$) in Magnet QB2.

<u>Pole</u>	<u>Normal</u>	<u>Skew</u>
6	6.33	6.01
8	-0.44	-1.70
10	0.59	-1.83
12	-0.95	0.84
14	0.88	0.31
16	0.01	0.00
18	0.51	0.59
20	-1.63	0.26
22	0.11	-0.03
24	-0.04	-0.11
26	-0.38	-0.50
28	0.60	-0.06
30	0.11	0.08

The deviation from a pure quadrupole field is shown in Fig. 3-13 on the next page. The normal sextupole component can be seen to dominate. There are also skew 8- and 10-poles and a normal 20-pole. The excitation dependence of the 12-pole is shown in Fig. 3-14, also on the next page. The center line of the hysteresis has become much flatter than in older quadrupoles. This means that the new collars have almost completely eliminated coil motion. The 12 pole is also measured with a Morgan coil and the two methods give similar results.

3.6 Statistical Analysis of Magnet Data

3.6.1 Dipoles. We have made 100 individual measurements on about 70 magnets. A statistical overview of the data is presented here.

Figure 3-15 is a histogram of quench currents in Magnet Test Facility measurements. The cooling conditions are all similar. The typical

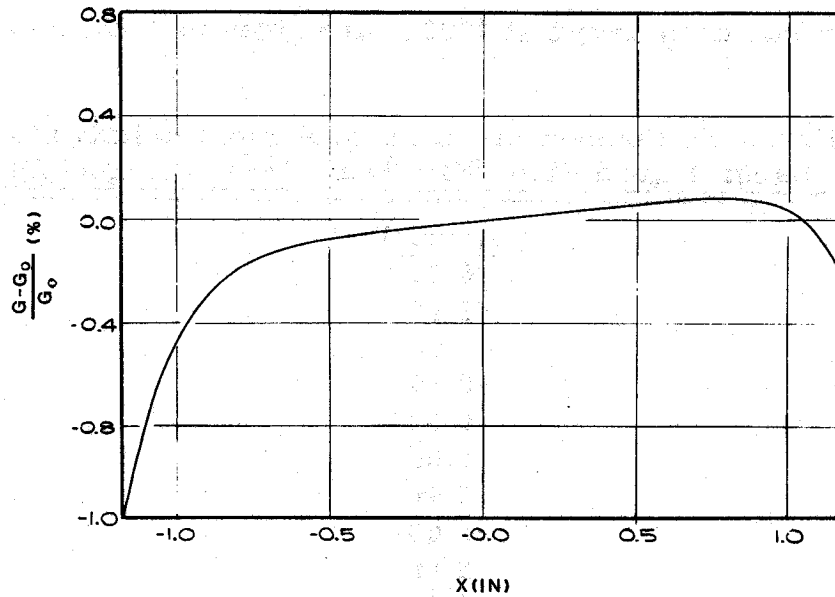


Fig. 3-13. Measured gradient distribution in QB2.

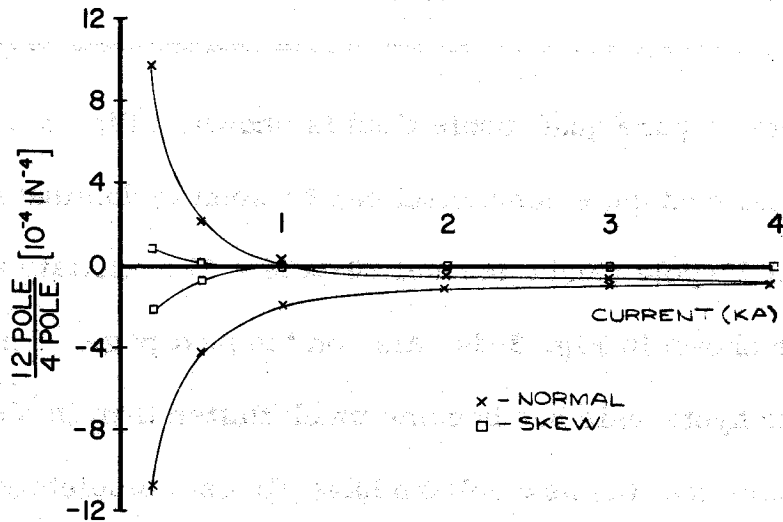


Fig. 3-14. Ratio of 12-pole to 4-pole field at 1 in. as a function of current in QB2.

temperature in the single phase is 4.7 K (± 0.1 K) and 4.55 K in the two-phase return. Usually the subcooling of the single phase is 3 psi and the mass flow is 20 to 30 g/s.

There have been noticeable changes in transfer ratios (G/A) with various collaring schemes, as shown in Fig. 3-16. The FWHM is

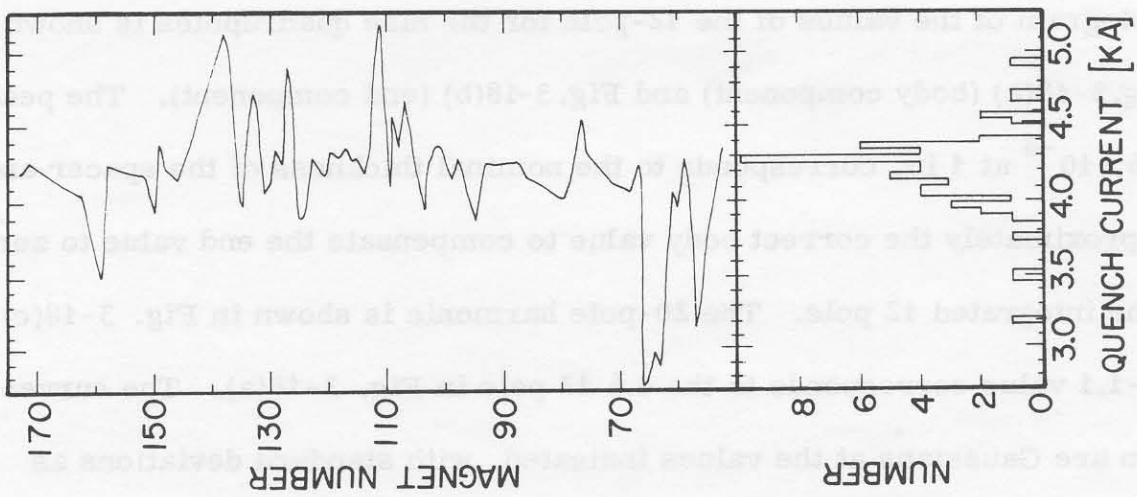


Fig. 3-15. Quench-current distribution over dipoles.

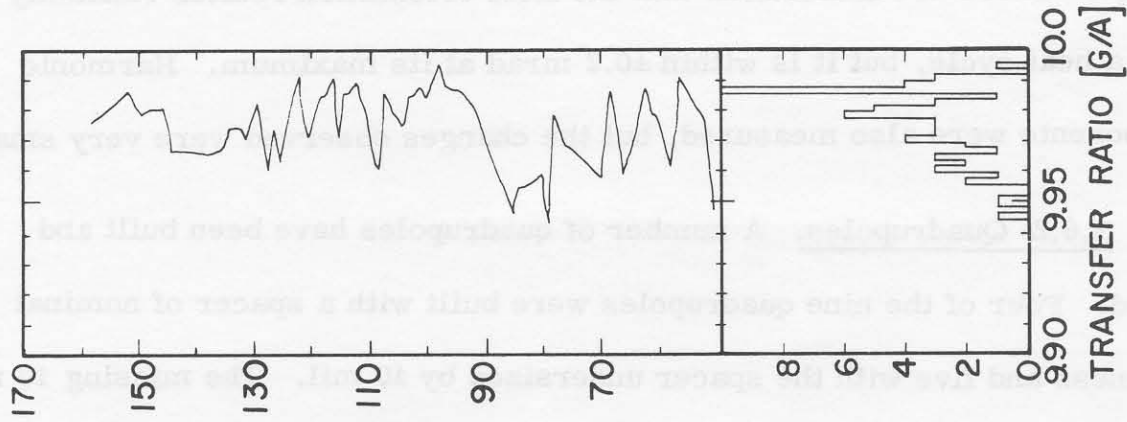


Fig. 3-16. Transfer-ratio distribution over dipoles.

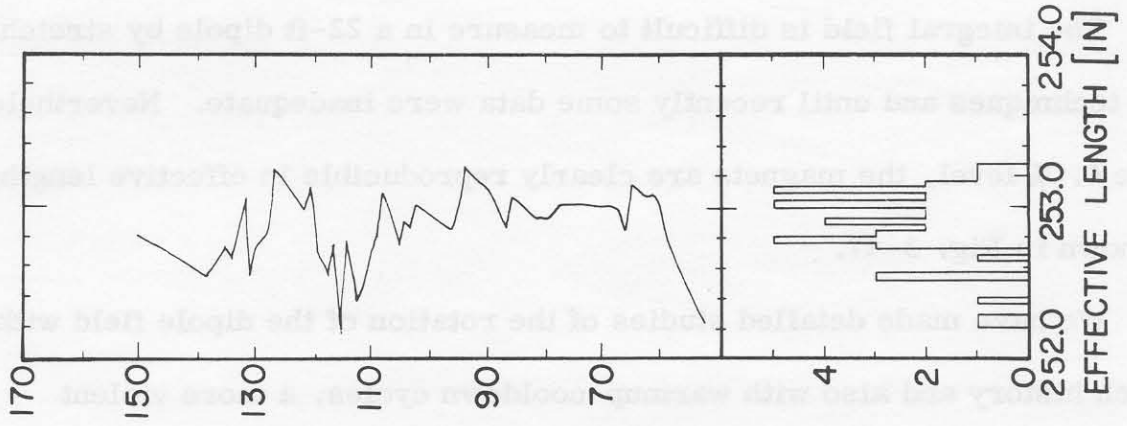


Fig. 3-17. Effective-length distribution over dipoles.

approximately 0.1% over all magnets measured, but bunching with smaller width can be perceived as a function of magnet number.

The integral field is difficult to measure in a 22-ft dipole by stretched-wire techniques and until recently some data were inadequate. Nevertheless, at the 0.1% level, the magnets are clearly reproducible in effective length, as shown in Fig. 3-17.

We have made detailed studies of the rotation of the dipole field with quench history and also with warmup-cooldown cycles, a more violent change. There are indications that the field orientation rotates randomly over a heat cycle, but it is within ± 0.2 mrad at its maximum. Harmonic components were also measured, but the changes observed were very small.

3.6.2 Quadrupoles. A number of quadrupoles have been built and tested. Four of the nine quadrupoles were built with a spacer of nominal thickness and five with the spacer undersized by 10 mil. The missing 10 mil was shimmed in on the other side of the coil shown in Fig. 3 - 5.

A histogram of the values of the 12-pole for the nine quadrupoles is shown in Fig.3-18(a) (body component) and Fig.3-18(b) (end component). The peak at 4.6×10^{-4} at 1 in. corresponds to the nominal thickness of the spacer and is approximately the correct body value to compensate the end value to zero for the integrated 12 pole. The 20-pole harmonic is shown in Fig. 3-18(c). The -1.1 value corresponds to the 4.6 12 pole in Fig. 3-18(a). The curves shown are Gaussians at the values indicated, with standard deviations as

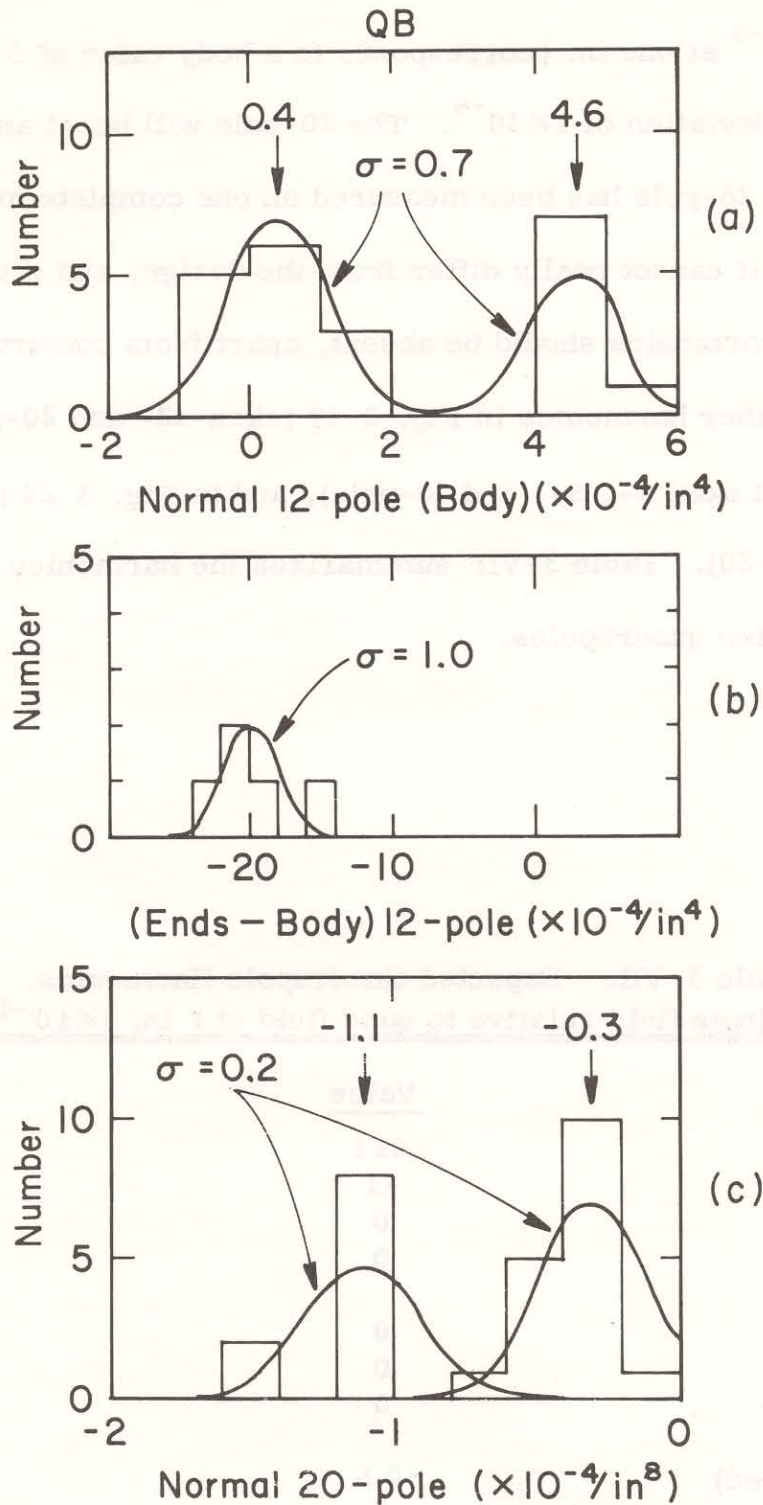


Fig. 3-18. Normal 12-pole and 20-pole distribution of quadrupoles. (Multipole field relative to quadrupole field at 1 in.)

shown. Thus we see that we can build quadrupoles with an integrated 12-pole of $(0\pm 1)\times 10^{-4}$ at one in. [corresponds to a body value of 5 in Fig. 3-18(a)] with a standard deviation of 1×10^{-4} . The 20-pole will be -1 and the 28-pole 0.6×10^{-4} . The 28-pole has been measured on one complete magnet to be about 0.7×10^{-4} ; it cannot really differ from the design, and it does not.

All other harmonics should be absent, apart from construction errors. We show these other harmonics in Fig. 3-19 (skew 12- and 20-pole), Fig. 3-20 (normal and skew 6-, 8-, and 10-pole), and in Fig. 3-21 (the integrated values of Fig. 3-20). Table 3-VII summarizes the harmonics expected in the final production quadrupoles.

Table 3-VII. Expected Quadrupole Harmonics.
Multipole field relative to quad field at 1 in. ($\times 10^{-4}/\text{in.}^{n-1}$)

	<u>Value</u>	<u>σ (per Q)</u>
Integral 12-pole	0 ± 1	< 1
Integral 20-pole	-1	0.2
Skew 12-pole	0	0.25
Skew 20-pole	0	0.05
Average 6-pole	0	< 4
Average 8-pole	0	1.7
Average 10-pole	0	1.0
28-pole (measured)	~ 0.6	-

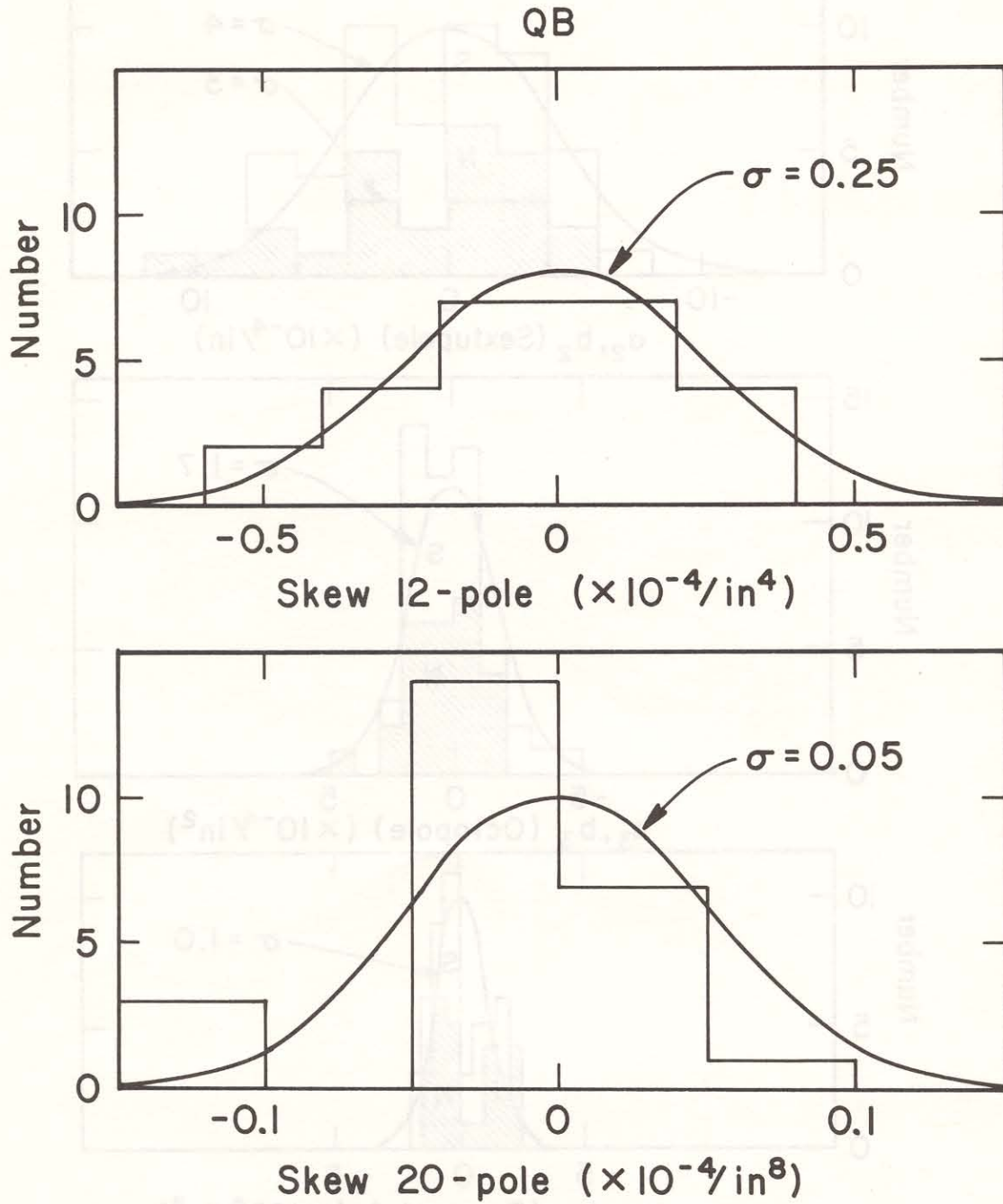


Fig. 3-19. Skew 12-pole and 20-pole distribution of quadrupoles.
(Multipole field relative to quadrupole field at 1 in.)

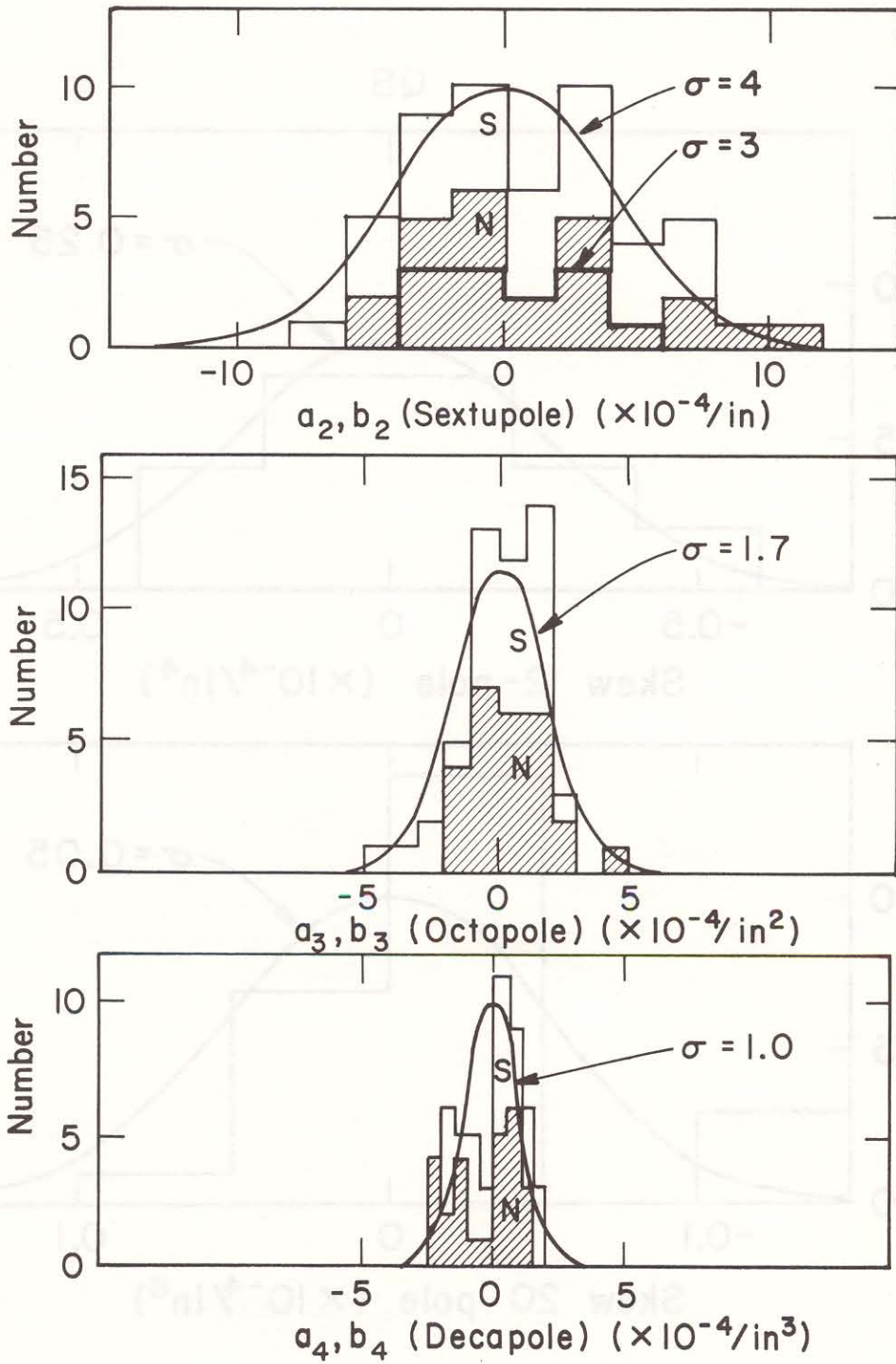


Fig. 3-20. 6-pole, 8-pole, and 10-pole distribution of quadrupoles. (Multipole field relative to quadrupole field at 1 in.)

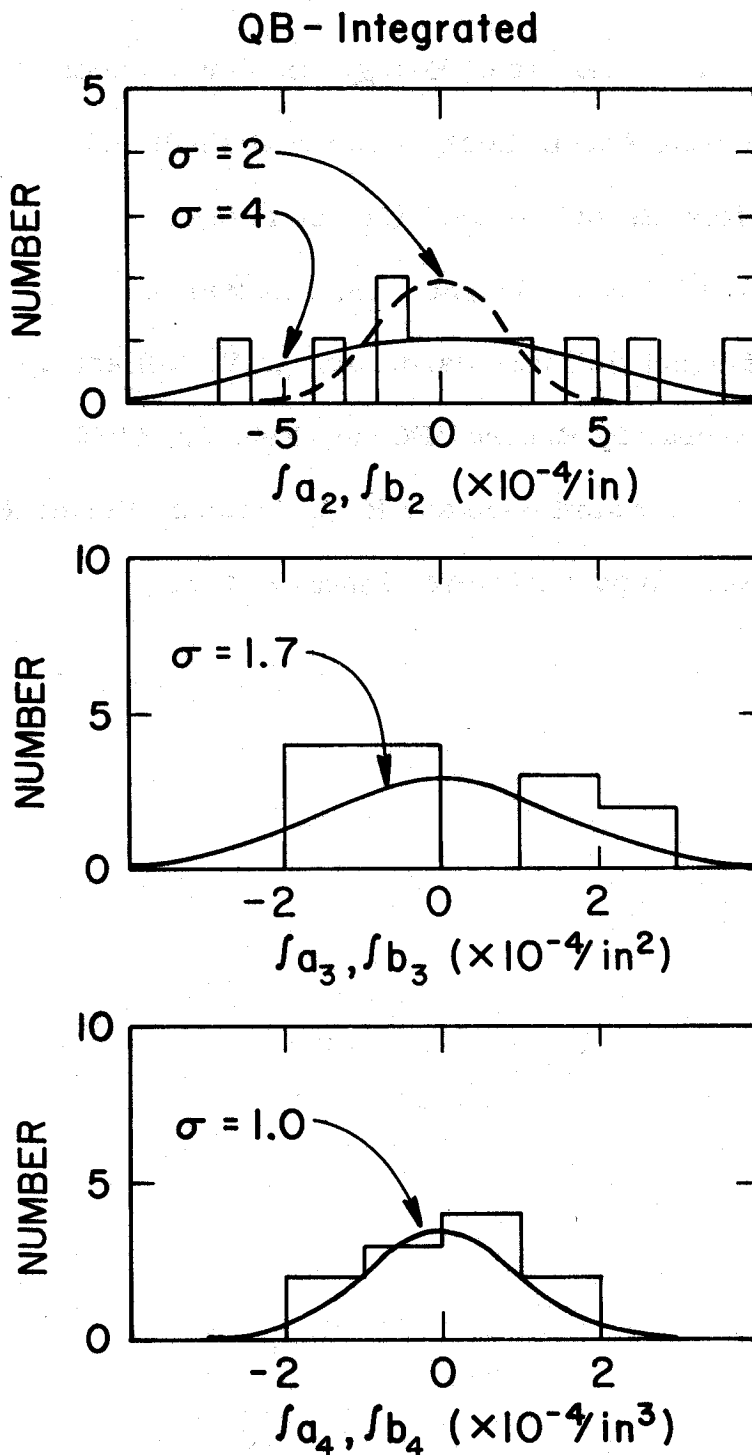


Fig. 3-21. Integrated 6-pole, 8-pole, and 10-pole distribution of quadrupoles. (Multipole field relative to quadrupole field at 1 in.)

References

- ¹Recent Measurement Results of Energy Doubler Magnets, M. Wake et al., Proc. 1979 Particle Accel. Conf. (to be published) and Fermi National Accel. Laboratory Report UPC-95 (March 1979).
- ²R. E. Peters, IEEE Trans. Magnets 15, 135 (1979).
- ³The Amateur Magnet Builders Handbook, A. V. Tollestrup, Fermi National Accelerator Laboratory Report UPC-86, Feb. 22, 1979.
- ⁴Quadrupoles, G. R. Kalbfleisch and R. E. Peters, Fermi National Accelerator Laboratory Report UPC-42, January, 1979.